Embedded Self-Sensing Piezoelectric Active Sensors for On-Line Structural Identification

Victor Giurgiutiu
Associate Professor, Mem. ASME
Department of Mechanical Engineering,
University of South Carolina,
Columbia, SC 29208
e-mail: victorg@sc.edu

Andrei N. Zagrai
Graduate Research Assistant,
Student Mem. ASME,
Department of Mechanical Engineering,
University of South Carolina,
Columbia, SC 29208

The benefits and limitations of using embedded piezoelectric active sensors for structural identification at ultrasonic frequency are highlighted. An analytical model based on structural vibration theory and theory of piezoelectricity was developed and used to predict the electro-mechanical (E/M) impedance response, as it would be measured at the piezoelectric active sensor's terminals. The model considers one-dimension structures and accounts for both axial and flexural vibrations. Experiments were conducted on simple specimens in support of the theoretical investigation, and on realistic turbine blade specimen to illustrate the method's potential. It was shown that E/M impedance spectrum recorded by the piezoelectric active sensor accurately represents the mechanical response of a structure. It was further proved that the response of the structure is not modified by the presence of the sensor, thus validating the latter's noninvasive characteristics. It is shown that such sensors, of negligible mass, can be permanently applied to the structure creating a nonintrusive sensor array adequate for on-line automatic structural identification and health monitoring. The sensor calibration procedure is outlined. Numerical estimation of the noninvasive properties of the proposed active sensors in comparison with conventional sensors is presented. Self-diagnostics capabilities of the proposed sensors were also investigated and methods for automatic self-test implementation are discussed. The paper underlines that the use of piezoelectric wafer active sensors is not only advantageous, but, in certain situations, may be the sole investigative option, as in the case of precision machinery, small but critical turbine-engine parts, and computer industry components.
[DOI: 10.1115/1.1421056]

1 Introduction

Modal analysis and dynamic structural identification have become an intrinsic part of current engineering practice. Structural frequencies, damping, and modes shapes identified through this process are subsequently used to predict dynamic response, avoid resonances, and even monitor structural change that are indicative of incipient failure [1].

Traditional modal analysis testing [2–4] relies on two essential components: (a) structural excitation; and (b) vibration pickups. Figure 1 shows that traditional structural excitation can be either harmonic sweep, or impulse. The former is more precise and can zoom in on resonant frequencies; the latter is more expedient and preferred for quick estimations. The vibration pickups can measure displacement, velocity, or acceleration. Current technologies cover miniaturized self-conditioning accelerometers [5] and laser velocimeters [6]. The accelerometers allow installation of sensor arrays that accurately and efficiently measure the mode shapes, while the laser offers contactless measurements that are essential for low mass sensitive structures. The disadvantages of accelerometers are cost, unavoidable bulkiness, and possible interference with the structural dynamics through their added mass. Laser velocimeters, on the other hand, need to scan the structure to measure the mode shapes, and this significantly increases the duration of the experiments.

The advent of commercially available low-cost piezoceramics has opened new opportunities for structural identification. Through their intrinsic electro-mechanical (E/M) coupling, the piezoceramics can act as both sensors and actuators. Additionally, their frequency bandwidth is orders of magnitude larger than that of conventional shakers and even impact hammers. Small piezoelectric (PZT) ceramic wafers can be permanently attached to structural surface. They could form sensor and actuator arrays that permit effective modal identification in a wide frequency band. Crawley and Luis [7] proposed the use of piezoceramic wafers as elements of intelligent structures. Dimitiradis et al. [8] and D'Cruz [9] used piezoelectric wafers for structural excitation. Zhou et al. [10] performed experiments in which a PZT wafer produced the excitation, while a laser velocimeter picked up the vibration response. Several investigators [11,12] used piezopolymer films for vibration sensing. Banks [13] describes experiments in which the PZT wafer was used initially for excitation, and then for sensing the free decay response. Wang and Chen [14] used a PZT wafer to excite the structure and an array of PVDF film sensors to pick up the forced vibration response and generate the frequencies and mode shapes through multi-point signal processing.

Liang et al. [15] performed the coupled E/M analysis of adaptive systems driven by a surface-attached piezoelectric wafer. The aim of the analysis was to determine the actuator power consumption and system energy transfer. A 1-degree of freedom (1-DOF) analysis was performed, and the electrical admittance as measure at the terminals of the PZT wafer attached to the structure was derived in the form:

$$Y(\omega) = i\omega C\left(1 - \kappa_{31}^2 \frac{Z_{str}(\omega)}{Z_{str}(\omega) + Z_A(\omega)}\right) \tag{1}$$

where C is the electrical capacitance of the PZT active sensor, $Z_{str}(\omega)$ is the 1-DOF structural impedance as seen by the sensor, and $Z_A(\omega)$ is the quasi-static impedance of the sensor. A 1-DOF numerical example was used to show that the E/M admittance response accurately reflects the system dynamic response. At coupled-system resonance, the real part of the E/M admittance was shown to have a distinct peak. However, due to the additional stiffness contributed by the PZT wafer, the system natural frequency shifted from 500 Hz (without PZT wafer) to 580 Hz (with PZT wafer). Experimental curve-fitting results were also pre-

Contributed by the Technical Committee on Vibration and Sound for publication in the JOURNAL OF VIBRATION AND ACOUSTICS. Manuscript received Feb. 2001; revised July 2001. Associate Editor: R. Ohayon.

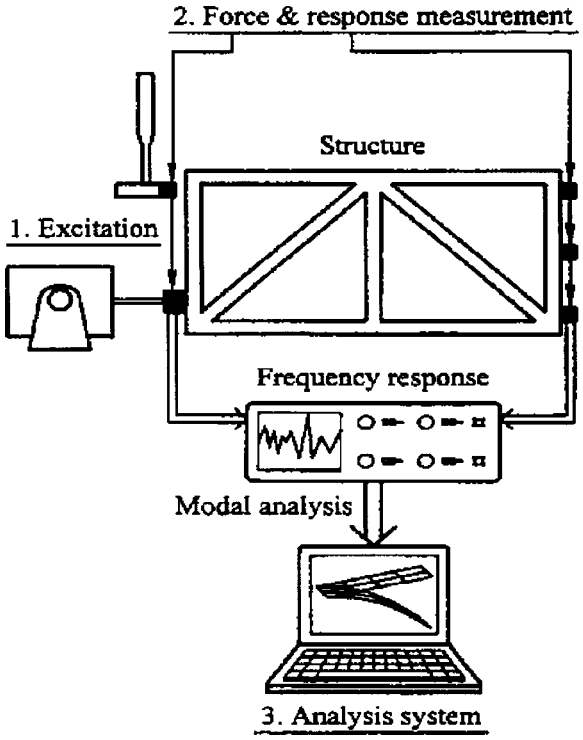

Fig. 1 Schematic of conventional modal analysis structural identification experiments (Heylen et al. 1997)

sented. No modeling of the structural substrate was included, and no prediction of $Z_{str}(\omega)$ for a multi-DOF structure was presented. This work was continued and extended by Sun et al. [16] who used the half-power bandwidth method to accurately determine the natural frequency values. Mode shape extraction methodology, using multiple sensors self and across admittances were explored. Experiments were performed on aluminum beams at frequencies up to 7 kHz. These two papers were the first to conceptualize that the E/M admittance as seen at the sensor terminals reflects the coupled-system dynamics, and that an embedded PZT wafer could be used as a structural-identification sensor. However, no theoretical modeling of the E/M impedance/admittance response for comparison with experimental data was attempted. Nor were the issues of sensor calibration, disbonding/self-diagnostics, and consistency examined.

Subsequently, several authors reported the use of the E/M impedance method for structural health monitoring, whereby the admittance or impedance frequency spectra of pristine and damaged structures were compared [17–20]. The method has been shown to be especially effective at ultrasonic frequencies, which properly capture the changes in local dynamics due to incipient structural damage. (Such changes are too small to affect the global dynamics and hence cannot be readily detected by conventional low-frequency vibration methods.) The method is direct and easy to implement, the only required equipment being an electrical impedance analyzer.

In contrast to the extensive experimental effort invested in this method, little theoretical work on its modeling has been reported to date. Park, Cudney, and Inman [21] showed that ''there is little analytical work done about the vibration modes of complex structures at ultrasonic frequencies'' and hence restricted their analysis to axial vibrations. In addition, only the structural displacement response was predicted. A few other investigators have attempted to model structures with piezoelectric active sensors [10,22,23], but none have derived explicit expressions for predicting the E/M admittance and impedance as it would be measured by the impedance analyzer at the embedded active sensor terminals during the structural identification process. Such a derivation is necessary to permit complete understanding of the phenomenon and to allow critical comparison with the abundant experimental results.

In response to this need, this work set forth to present a step-by-step derivation of the interaction between the piezoelectric active sensor and the host structure, and to produce, for the first time, analytical expressions and numerical results for the E/M admittance and impedance seen at sensor terminal. These numerical results are then directly compared with those experimentally measured at the piezoelectric active sensor terminals during the structural identification process. In our derivation, the limitations of the quasi-static sensor approximation adopted by previous investigators are lifted. Exact analytical expressions are being used for structural modeling of simultaneous axial and flexural vibrations. Free-free boundary conditions that can unequivocally be implemented during experimental testing (though more difficult to model) are being used.

To verify the theoretical model, experiments were conducted on miniature metallic beam specimens. The E/M admittance and impedance were captured in the 1-30 kHz range, and compared with theoretical predictions. For the first time, a direct comparison between the modeled and measured E/M admittance spectra are presented, and the capabilities and limitations of the piezoelectric active sensors to detect the structural resonance frequencies from the E/M admittance response are rationally evaluated. The result of this comparison proved that embedded piezoelectric active sensors could reliably perform structural identification. Their usefulness is especially apparent in the ultrasonic range and beyond, where conventional sensors loose their effectiveness.

In our work, small unobtrusive active sensors that do not effectively modify the structural stiffness and faithfully measure the structural dynamics were used. The active sensors are orders of magnitude below the structural stiffness and mass. Because the sensors are small and unobtrusive, the dynamics of the host structure is not affected by the sensor presence, and accurate structural identification is possible.

Another important aspect covered in this work is that of sensor calibration, reliability and repeatability. These aspects are essential for the qualification of new sensor concepts. We statistically studied the intrinsic properties of the piezoelectric active sensors in the as received condition (single wafers), and after adhesive attachment to the structure. Good consistency and repeatability was found in both situations. In addition, in order to prevent false readings during long-service usage of these sensors, we have explored and experimentally verified sensor self-test procedures that are able to identify in-situ sensor debonding.

2 Analytical Model

Consider a 1-D structure with a PZT active sensor attached to it's surface [Fig 2(*a*)]. The PZT active sensor has length l_a, and lies between x_a and x_a+l_a. Upon activation, the PZT active sensor expands by ε_{PZT}. This generates a reaction force F_{PZT} from the beam onto the PZT and an equal and opposite force from the PZT onto the beam [Fig 2(*b*)]. This force excites the beam. At the neutral axis, the effect is felt as an axial force excitation, N_{PZT}, and a bending moment excitation, M_{PZT}. As the active sensor is electrically excited with a high-frequency harmonic signal, it will induce elastic waves into the beam structure. The elastic waves travel sideways into the beam structure, and set it up into oscillation. In a steady-state regime, the structure oscillates at the PZT excitation frequency. The reaction force per unit displacement (dynamic stiffness) presented by the structure to the PZT will depend on the internal state of the structure, on the excitation frequency, and on the boundary conditions:

$$k_{str}(\omega)=\hat{F}_{PZT}(\omega)/\hat{u}_{PZT}(\omega), \tag{2}$$

where $\hat{u}_{PZT}(\omega)$ is the displacement amplitude at frequency ω, $\hat{F}_{PZT}(\omega)$ is the reaction force, and $k_{str}(\omega)$ is the dynamic stiff-

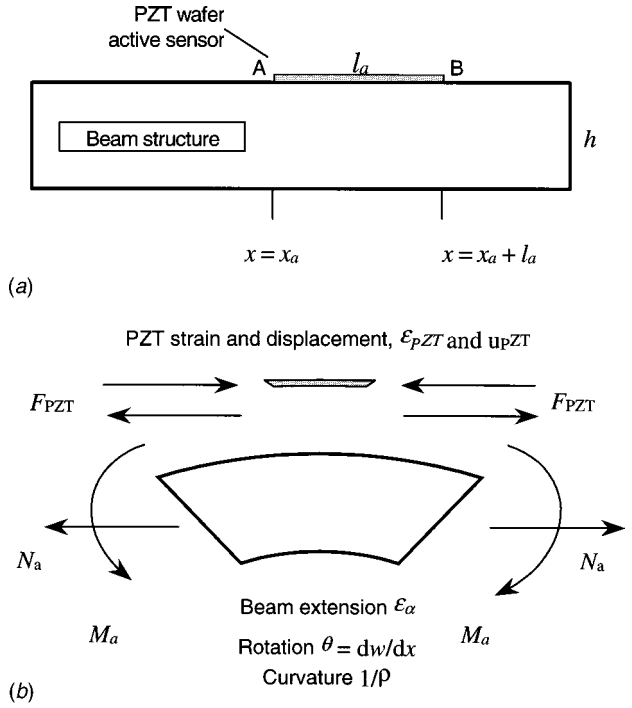

Fig. 2 Interaction between PZT active sensor and a substructure: (*a*) geometry; (*b*) forces and moments

ness. The symbol ˆ signifies amplitude. Since the size of the PZT is very small with respect to the size of the structure, formula (2) represents a point-wise structural stiffness.

2.1 Elastically Constrained PZT Active Sensor. Consider a PZT wafer of length l_a, thickness t_a, and width b_a, undergoing longitudinal expansion, u_1, induced by the thickness polarization electric field, E_3. The electric field is produced by the application of a harmonic voltage $V(t)=\hat{V}e^{i\omega t}$ between the top and bottom surfaces (electrodes). The resulting electric field, $E=V/t$, is assumed uniform with $x_1(\partial E/\partial x_1=0)$. The length, width, and thickness are assumed to have widely separated values ($t_a \ll b_a \ll l_a$) such that the length, width, and thickness motions are practically uncoupled.

The constitutive equations of the PZT material are:

$$S_1 = s_{11}^E T_1 + d_{31} E_3 . \tag{3}$$

$$D_3 = d_{31} T_1 + \varepsilon_{33}^T E_3 . \tag{4}$$

where S_1 is the strain, T_1 is the stress, D_3 is the electrical displacement (charge per unit area), s_{11}^E is the mechanical compliance at zero field, ε_3^T is the dielectric constant at zero stress, d_{31} is the induced strain coefficient, i.e., mechanical strain per unit electric field.

Since the piezoelectric active sensor is ultimately bonded to the structure, we consider an elastically constrained sensor for further analysis. As the result of this assumption, an active sensor is constrained by structural stiffness, k_{str}, as shown in Fig. 3. For symmetry, the structural stiffness has been split into two end components, each of size $2k_{str}$. The boundary conditions applied at both ends connect the resultant of internal stresses with the spring reaction force, i.e.,

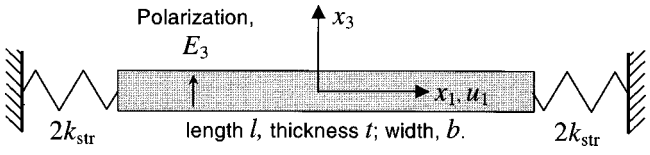

Fig. 3 PZT wafer active sensor constrained by structural stiffness, k_{str}

$$\begin{aligned} T_1\left(\frac{1}{2}\,l_a\right) b_a t_a &= -2k_{str} u_1\left(\frac{1}{2}\,l_a\right) \\ T_1\left(-\frac{1}{2}\,l_a\right) b_a t_a &= 2k_{str} u_1\left(-\frac{1}{2}\,l_a\right) \end{aligned} \tag{5}$$

Substitution of Eq. (5) into Eq. (3) gives:

$$\begin{aligned} u_1'\left(\frac{1}{2}\,l_a\right) b_a t_a &= -2k_{str}\frac{s_{11}^E}{bt}\, u_1\left(\frac{1}{2}\,l_a\right) + d_{31}E_3 \\ u_1'\left(-\frac{1}{2}\,l_a\right) b_a t_a &= 2k_{str}\frac{s_{11}^E}{bt}\, u_1\left(-\frac{1}{2}\,l_a\right) + d_{31}E_3 \end{aligned} \tag{6}$$

Introducing the quasi-static stiffness of the PZT active sensor,

$$k_{PZT} = \frac{A_a}{s_{11}^E l_a}, \tag{7}$$

and the stiffness ratio

$$r = \frac{k_{str}}{k_{PZT}}, \tag{8}$$

Now Eq. (6) can be re-arranged in the form:

$$u_1'\left(\pm\frac{1}{2}\,l_a\right) b_a t_a \pm \frac{r}{l_a/2}\cdot u_1\left(\frac{1}{2}\,l_a\right) = d_{31}E_3 \tag{9}$$

Mechanical Response

Using Newton's law of motion, $T_1' = \rho\ddot{u}_1$, and the strain-displacement relation, $S_1 = u_1'$, Eq. (3) yields the axial waves equation:

$$\ddot{u}_1 = c_a^2 u_1'' \tag{10}$$

where $(\dot{}) = \partial(\,)/\partial t$, and $(\,)' = \partial(\,)/\partial x$, while $c_a^2 = 1/\rho s_{11}^E$ is the sound speed. The general solution of Eq. (10) is:

$$u_1(x,t) = \hat{u}_1(x)e^{i\omega t} \quad \text{where} \quad \hat{u}_1(x) = (C_1 \sin\gamma x + C_2 \cos\gamma x) \tag{11}$$

The variable $\gamma = \omega/c_a$ is the wave number [24], and (ˆ) signifies the harmonic motion amplitude. The constants C_1 and C_2 are to be determined from the boundary conditions.

Substitution of the general solution (11) yields the following linear system in C_1 and C_2:

$$\begin{aligned} (\varphi\cos\varphi + r\sin\varphi)C_1 - (\varphi\sin\varphi - r\cos\varphi)C_2 &= \frac{1}{2}\,u_{ISA} \\ (\varphi\cos\varphi + r\sin\varphi)C_1 + (\varphi\sin\varphi - r\cos\varphi)C_2 &= \frac{1}{2}u_{ISA} \end{aligned} \tag{12}$$

where $u_{ISA} = d_{31}\hat{E}_3 \cdot l_a$ and $\varphi = 1/2\ \gamma l_a$. Upon solution,

$$\hat{u}_1(x) = \frac{1}{2}u_{ISA}\frac{\sin\gamma x}{(\varphi\cos\varphi + r\sin\varphi)} \tag{13}$$

Electrical Response

Equation (4) can be re-expressed as:

$$D_3 = \frac{d_{31}}{s_{11}^E}(u_1' - d_{31}E_3) + \varepsilon_{33}^T E_3 = \varepsilon_{33}^T E_3\left[1 + \kappa_{31}^2\left(\frac{u_1'}{d_{31}E_3} - 1\right)\right] \tag{14}$$

where $\kappa_{13}^2 = d_{31}^2/(s_{11}^E\varepsilon_{33})$ is the E/M coupling factor [25]. Integration of Eq. (14) yields the charge:

$$Q=\int_{-(l_a/2)}^{+(l_a/2)}\int_{-(b_a/2)}^{+(b_a/2)} D_3\,dx\,dy$$

$$=\varepsilon_{33}^{T}\frac{b_a l_a}{t}\,V\left[1+\kappa_{31}^2\left(\frac{1}{l_a}\frac{1}{d_{31}E_3}u_1\Big|_{-\frac{l_a}{2}}^{+\frac{l_a}{2}}-1\right)\right] \tag{15}$$

where $\varepsilon_{33}^{T}b_a l_a/t_a=C$ is the conventional capacitance of the piezoelectric wafer. For harmonic motion, $\hat{I}=\mathrm{i}\omega\cdot\hat{Q}$. Recall the expressions $Y=\hat{I}/\hat{V}$ and $Z=Y^{-1}$ for the electric admittance and impedance, we arrive to admittance and impedance expressions for a PZT active sensor constrained by the structural substrate with an equivalent stiffness ratio r:

$$Y=\mathrm{i}\omega\cdot C\left[1-\kappa_{31}^2\left(1-\frac{1}{\varphi\cot\varphi+r}\right)\right]$$
$$Z=\frac{1}{\mathrm{i}\omega\cdot C}\left[1-\kappa_{31}^2\left(1-\frac{1}{\varphi\cot\varphi+r}\right)\right]^{-1} \tag{16}$$

In this equation the structural stiffness ratio, r, is additive to the sensor resonance term, $\varphi\cot\varphi$. When the PZT active sensor is used in a frequency sweep, the apparent structural stiffness, k_{str} will vary with frequency, going through zero at structural resonances, and extreme values at structural anti-resonances. Equations (16) infer that both structural resonances and sensor resonances will be reflected in the admittance and impedance frequency spectra.

Analysis of the asymptotic behavior of Eqs. (16) reveals important facts., As $r\to 0$, i.e., vibrations of a free-free sensor, we get $Y_{free}=\mathrm{i}\omega\cdot C[1-\kappa_{31}^2(1-1/\varphi\cot\varphi)]$. For $r\to\infty$, i.e., vibrations of a clamped sensor, we get $Y_{clamped}=\mathrm{i}\omega\cdot C[1-\kappa_{31}^2]$. Both these formulas are consistent with the fundamental theory of piezoelectricity [26]. On the other hand, as $\gamma l_a\to 0$ (i.e., quasi-static sensor conditions), we get:

$$Y=\mathrm{i}\omega\cdot C\left[1-\kappa_{31}^2\frac{r}{1+r}\right],\quad Z=\frac{1}{\mathrm{i}\omega\cdot C}\left[1-\kappa_{31}^2\frac{r}{1+r}\right]^{-1}, \tag{17}$$

which is consistent with the results of Liang et al. [15], Giurgiutiu et al. [27,28], and other investigators. The expressions contained in Eqs. (16) are a generalization of these results and bridge the gap between high-frequency sensor-focused analysis (e.g., [26]) and low-frequency structure-focused analysis (e.g., [15]). The present results cover the complete frequency spectrum and encompass both structure and sensor dynamics.

The effect of structural and sensor damping can be easily introduced in Eqs. (16) by the use of complex notations:

$$\overline{Y}=\mathrm{i}\omega\cdot\overline{C}\left[1-\overline{\kappa}_{31}^2\left(1-\frac{1}{\overline{\varphi}\cot\overline{\varphi}+\overline{r}}\right)\right]$$
$$\overline{Z}=\frac{1}{\mathrm{i}\omega\cdot\overline{C}}\left[1-\overline{\kappa}_{31}^2\left(-\frac{1}{\overline{\overline{\varphi}\cot\overline{\varphi}+\overline{r}}}\right)\right]^{-1} \tag{18}$$

where $\overline{r}$ is the frequency-dependent complex stiffness ratio that reflects the structural point-wise dynamics and the sensor dissipation mechanisms.

2.2 Dynamics of the Structural Substrate. The response of the structural substrate to the PZT excitation is deduced from the general theory of beam vibrations [29–32]. However, the PZT excitation departs from the typical textbook formulation since it acts as a pair of self-equilibrating axial forces and bending moments that are separated by a small finite distance, l_{PZT}. This feature gives *gusto* to our analysis.

Definition of the Excitation Forces and Moments

The excitation forces and moments acting upon the beam structure are derived from the PZT force, $F_{PZT}=\hat{F}_{PZT}e^{i\omega t}$, using the beam cross-section geometry [Fig. 2(b)]:

$$M_a=F_{PZT}\frac{h}{2},\quad N_a=F_{PZT} \tag{19}$$

The space-wise distribution of excitation bending moment and axial force are expressed using the Heaviside function, $H(x-x_a)$, defined as $H(x-x_a)=0$ for $x<x_a$, and $H(x-x_a)=1$ for $x_a\leqslant x$:

$$N_e(x,t)=N_a[-H(x-x_a)+H(x-x_a-l_a)]\cdot e^{i\omega t} \tag{20}$$

$$M_e(x,t)=-M_a[-H(x-x_a)+H(x-x_a-l_a)]\cdot e^{i\omega t} \tag{21}$$

Equations (20) and (21) correspond to axial and flexural vibrations, respectively. Axial vibrations modes are usually of much larger frequency than flexural vibration modes, and were neglected by previous researchers [15]. However, their vibration frequencies are commensurable with those of the PZT active sensors. Other researchers have only considered axial modes and neglected the flexural vibrations [21]. In the present analysis, both axial and flexural vibrations are considered.

Axial Vibrations

The equation of motion for axial vibrations [30] is:

$$\rho A\cdot\ddot{u}(x,t)-EA\cdot u''(x,t)=N_e'(x,t) \tag{22}$$

Assume modal expansion

$$u(x,t)=\sum_{n=0}^{\infty} C_n X_n(x)\cdot e^{\mathrm{i}\omega t}, \tag{23}$$

where $X_n(x)$ are orthonormal mode shapes, i.e., $\int X_m X_n dx=\delta_{mn}$, with $\delta_{mn}=1$ for $m=n$, and 0 otherwise. C_n are the modal amplitudes. Substitution of Eq. (20) into (22) yields:

$$\rho A\cdot\ddot{u}(x,t)-EA\cdot u''(x,t)=\hat{N}_a[-\delta(x-x_a)+\delta(x-x_a-l_a)]\cdot e^{i\omega t} \tag{24}$$

where δ is Dirac's function. Since the mode shapes satisfy the free-vibration differential equation $EA\cdot X_n''+\omega_n^2\cdot\rho A\cdot X_n=0$, multiplication by $X_n(x)$ and integration over the length of the beam yields:

$$C_n=\frac{1}{\omega_n^2-\omega^2}\cdot\frac{\hat{N}_a}{\rho A}[-X(x_a)+X(x_a+l_a)] \tag{25}$$

Hence,

$$u(x,t)=\frac{\hat{N}_a}{\rho A}\sum_{n=0}^{\infty}\frac{-X_n(x_a)+X_n(x_a+l_a)}{\omega_n^2-\omega^2}\cdot X_n(x)\cdot e^{\mathrm{i}\omega t}, \tag{26}$$

Flexural Vibrations

For Euler-Bernoulli beams, the equation of motion under moment excitation is:

$$\rho A\cdot\ddot{w}(x,t)-EI\cdot w''''(x,t)=-M_e''(x,t) \tag{27}$$

Substitution of Eq. (21) into (27) yields:

$$\rho A\cdot\ddot{w}(x,t)+EI\cdot w''''(x,t)$$
$$=\hat{M}_a[-\delta'(x-x_a)+\delta'(x-x_a-l_a)]\cdot e^{i\omega t} \tag{28}$$

where δ' is the first derivative of Dirac's function ($\delta'=H''$). Assume modal expansion $w(x,t)=\sum_{n=N_1}^{N_2}C_n X_n(x)\cdot e^{i\omega t}$, where $X_n(x)$ are the orthonormal bending mode shapes, and N_1, N_2 are the mode numbers enduring the frequency band of interest. Since the mode shapes satisfy the free-vibration differential equation $EI\cdot X_n''''=\omega_n^2\cdot\rho A\cdot X_n$, multiplication by $X_n(x)$ and integration over the length of the beam yields:

$$C_n=\frac{1}{\omega_n^2-\omega^2}\cdot\frac{\hat{M}_a}{\rho A}\int_0^l X_n(x)[\delta'(x-x_a)-\delta'(x-x_a-l_a)]\mathrm{d}x \tag{29}$$

Integration by parts and substitution into the modal expansion expression yields

$$C_n=-\frac{1}{(\omega_n^2-\omega^2)}\frac{\hat{M}_a}{\rho A}[-X_n'(x_a)+X_n'(x_a+l_a)] \tag{30}$$

Hence,

$$w(x,t)=-\frac{\hat{M}_a}{\rho A}\sum_{n=1}^{\infty}\frac{-X_n'(x_a)+X_n'(x_a+l_a)}{\omega_n^2-\omega^2}\cdot e^{i\omega t} \tag{31}$$

Calculation of Frequency Response Function and Dynamic Structural Stiffness

To obtain the dynamic structural stiffness, k_{str}, presented by the structure to the PZT, we first calculate the elongation between the two points, A and B, connected to the PZT ends. Simple kinematics gives the horizontal displacement of a generic point P place on the surface of the beam:

$$u_P(t)=u(x)-\frac{h}{2}w'(x), \tag{32}$$

where u and w are the axial and bending displacements of the neutral axis. Letting P be A and B, and taking the difference, yields:

$$\begin{aligned}u_{PZT}(t)&=u_B(t)-u_A(t)\\&=u(x_a,t)-u(x_a+l_a,t)-\frac{h}{2}[w'(x_a,t)-w'(x_a+l_a,t)]\end{aligned} \tag{33}$$

Using Eqs. (19), (26), and (31), the amplitude of Eq. (33) becomes

$$\hat{u}_{PZT}=\frac{\hat{F}_{PZT}}{\rho A}\left\{\sum_{n_u}\frac{[U_{n_u}(x_a+l_a)-U_{n_u}(x_a)]^2}{\omega_{n_u}^2-\omega^2}+\left(\frac{h}{2}\right)^2\sum_{n_w}\frac{[W_{n_w}'(x_a+l_a)-W_{n_w}'(x_a)]^2}{\omega_{n_w}^2-\omega^2}\right\} \tag{34}$$

where differentiation between axial and flexural vibrations frequencies and mode shapes was achieved by the use of n_u, ω_{n_u}, $U_{n_u}(x)$ and n_w, ω_{n_w}, $W_{n_w}(x)$, respectively. Dividing Eq. (34) by $\hat{F}_{PZT}$ yields the structural frequency response function (FRF) to the Single Input Single Output (SISO) excitation applied by the PZT active sensor. This situation is similar to conventional modal testing [1] with the proviso that the PZT wafers are unobtrusive and permanently attached to the structure. For convenience, the axial and flexural components of the structural FRF are expressed separately, i.e.,

$$H_u(\omega)=\frac{1}{\rho A}\sum_{n_u}\frac{[U_{n_u}(x_a+l_a)-U_{n_u}(x_a)]^2}{\omega_{n_u}^2+2\mathrm{i}\zeta_{n_u}-\omega^2}, \tag{35}$$

$$H_w(\omega)=\frac{1}{\rho A}\left(\frac{h}{2}\right)^2\sum_{n_w}\frac{[W_{n_w}'(x_a+l_a)-W_{n_w}'(x_a)]^2}{\omega_{n_w}^2+2\mathrm{i}\zeta_{n_w}-\omega^2} \tag{36}$$

Modal damping, ζ, was introduced to provide practical veridicality to our modeling. The FRF's are additive, and the total FRF is simply

$$H(\omega)=H_u(\omega)+H_w(\omega) \tag{37}$$

The SISO FRF is the same as the dynamic structural compliance, as seen by the PZT wafer active sensor. The dynamic structural stiffness is the inverse of the structural compliance, i.e.,

$$k_{str}(\omega)=\frac{\hat{F}_{PZT}}{\hat{u}_{PZT}}=\rho A\left\{\sum_{n_u}\frac{[U_{n_u}(x_a+l_a)-U_{n_u}(x_a)]^2}{\omega_{n_u}^2+2\mathrm{i}\zeta_{n_u}-\omega^2}+\left(\frac{h}{2}\right)^2\sum_{n_w}\frac{[W_{n_w}'(x_a+l_a)-W_{n_w}'(x_a)]^2}{\omega_{n_w}^2+2\mathrm{i}\zeta_{n_w}-\omega^2}\right\}^{-1} \tag{38}$$

For free-free beams [31] axial and flexural components:

$$U_{n_u}(x)=A_{n_u}\cos(\gamma_{n_u}x),\quad A_{n_u}=\sqrt{2/l},\quad \gamma_{n_u}=\frac{n_u\pi}{l},$$

$$\omega_{n_u}=\gamma_{n_u}c,\quad c=\sqrt{\frac{E}{\rho}},\quad n_u=1,2,\ldots \tag{39}$$

$$W_{n_w}(x)=A_{n_w}[\cosh\gamma_{n_w}x+\cos\gamma_{n_w}x-\sigma_{n_w}\times(\sinh\gamma_{n_w}x+\sin\gamma_{n_w}x)]$$

$$\omega_{n_w}=\gamma_{n_w}^2a,\quad a=\sqrt{\frac{EI}{\rho A}},\quad A_{n_w}=1/\sqrt{\int_0^l W_{n_w}^2(x)dx}. \tag{40}$$

Numerical values of $l\cdot\gamma_{n_w}$ and σ_{n_w} for $n_w\leqslant 5$ can be found in Blevins [33], page 108; for $5<n_w$, $\gamma_{n_w}=1/l(2n+1)\pi/2$ and $\sigma_{n_w}=1$.

The derivations (18), (38), (39), (40) open the way for the numerical example and comparison with theoretical and experimental results.

3 Numerical Simulation and Experimental Results

The discussed analytical model was used to perform several numerical simulations that directly predict the E/M impedance and admittance signature at an active sensor's terminals during structural identification. Subsequently, experiments were performed to verify these predictions. The simulation conditions identically represent the real specimens consisted of small steel beams ($E=200$ GPa, $\rho=7750$ kg/m^3) of various thickness and widths fabricated in the laboratory. All beams were $l=100$ mm long with various widths $b_1=8$ mm (narrow beams) and $b_2=19.6$ mm (wide beams). The nominal thickness of the specimen was $h_1=2.6$ mm; by gluing two specimens back-to-back, we were also able to create double thickness specimens $h_2=5.2$ mm. Thus, four beam types were used (Fig. 4): narrow-thin, narrow-thick, wide-thin, and wide-thick. The comparison of wide and narrow beams was aimed at identifying the width effects in the frequencies spectrum, while the change from double to simple thickness was aimed at simulating the effect of corrosion (for traditional structures) and disbonding/delamination on adhesively bonded and composite structures. All specimens were instru-

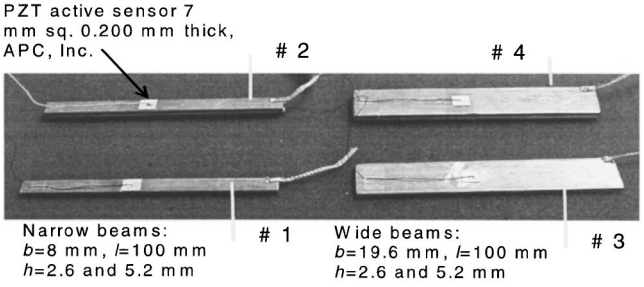

Fig. 4 Experimental specimens to simulate one-dimensional structure

Table 1 Theoretical and experimental results for wide and narrow beams with single and double thickness

#	Beam #1 (narrow thin)			Beam #2 (narrow thick)			Beam #3 (wide thin)			Beam #4 (wide thick)		
	Calc., kHz	Exp, kHz	Δ%	Calc., kHz	Exp, kHz	Δ%	Calc., kHz	Exp, kHz	Δ%	Calc., kHz	Exp, kHz	Δ%
1	1.396	1.390	-0.4	2.847	2.812	-1.2	1.390	1.363	-1.9	2.790	2.777	-0.5
2	3.850	3.795	-1.4	7.847	7.453	-5.2	3.831	3.755	-2	7.689	7.435	-3.4
3	7.547	7.4025	-2	15.383	13.905	-10.6	7.510	7.380	-1.7	15.074	13.925	-8.2
4	12.475	12.140	-2.7		20.650		12.414	12.093	-2.6		21.825	
5	18.635	17.980	-3.6	25.430	21.787	-16.7	18.545	17.965	-3.2	24.918	22.163	-12.4
6		24.840						24.852				
7	26.035	26.317	1	26.035	26.157	0.5	26.022	26.085	0.2	25.944	26.100	0.6
		Cluster 175 kHz			Cluster 210 kHz			Cluster 35 kHz			Cluster 60 kHz	

mented with thin 7-mm square PZT active sensors ($l_a=7$ mm, $b_a=7$ mm, $t_a=0.22$ mm) placed at $x_a=40$ mm from one end.

The numerical simulation was performed using a MathCAD-coded simulation based on modal analysis theory presented in previous sections assuming damping coefficient $\zeta=1$ percent for steel beams. Numerically exact expression for the axial and flexural frequencies and mode shapes were used [33]. The simulation was performed over a modal subspace that incorporates all modal frequencies in the frequency bandwidth of interest. The theoretical analysis indicates that these frequencies should be identical with the basic beam resonances, as predicted by classical vibration analysis [31]. ''Calc.'' columns of Table 1. show the first 6 predicted resonances for axial and flexural vibrations. The experimental set up is shown on Fig. 5. During the experiments, recording of the E/M impedance real part spectrum with the HP 4194A Impedance Analyzer was performed in the 1–30 kHz range. To approximate the free-free boundary conditions, the beams were supported on common packing foam. The beam natural frequencies were identified from the E/M impedance spectrum. The results are given in the ''Exp.'' columns of Table 1. It should be noted that the errors are small, and within the range normally accepted in experimental modal analysis. When the beam thickness was doubled, the frequencies also doubled. This is consistent with theoretical prediction. However, the error between theory and experiment seems larger for the double thickness beam, which may be caused by the compliance of the adhesive layer used in the construction of the double thickness beam. Even so, the confirmation of theoretical predictions by the experimental results is quite clear. The effect of beam width is demonstrated by comparison of ''Narrow Beam'' and ''Wide Beam'' columns in Table 1. The experimental results indicate cluster of frequencies, which move to higher frequencies as the width of the beam is reduced. We associate these clusters with width vibrations, which are not covered by the simple 1-D beam theory.

The width vibrations are also influenced by the thickness, i.e., they shift to higher frequencies as the thickness is increased. This is also noticeable in Table 1, which shows that the lowest cluster appeared for single thickness wide specimen and the highest cluster for double thickness narrow beam. Another important aspect that needs to be noticed is that the first axial mode of vibrations is at 25 kHz. This explains the ~25 KHz double frequencies observed in the single-thickness beams, both narrow and wide. An example of the actual impedance spectra is given in Figs. 6–9. The calculated and measured results are shown superposed. It was found that for the first 4 modes of single thickness beams, the predicted and measured frequency values almost superpose. For the 5th mode, there is a slight difference.

These results prove again that the predicted and measured results are in close agreement, well within the tolerance normally expected from experimental modal analysis. The results obtained for double thickness beams are less precise due to inhomogeneity introduced by the layer of glue between single thickness beams. This inhomogeneity found to alter E/M impedance response of a beam.

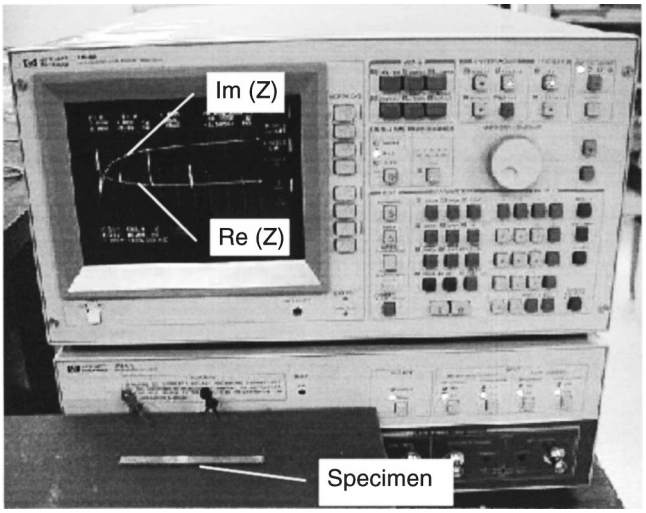

Fig. 5 Experimental set up for dynamic identification of steel beams

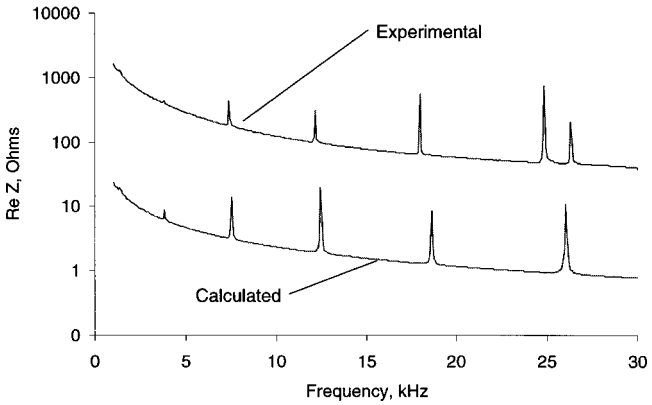

Fig. 6 Experimental and calculated spectra of frequencies for single thickness narrow beam (Beam #1)

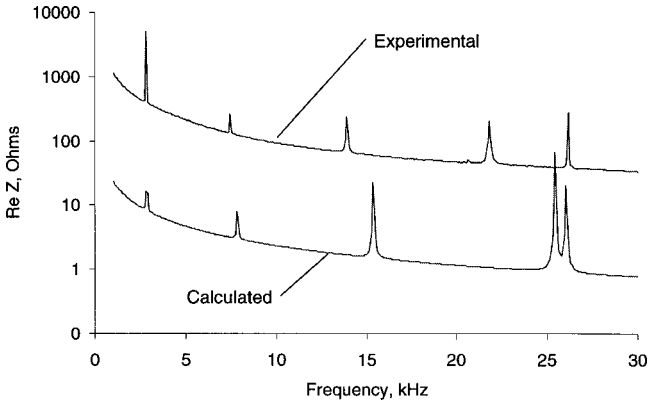

Fig. 7 Experimental and calculated spectra of frequencies for double thickness narrow beam (Beam #2)

3.1 Comparison with Conventional Methods. In order to highlight the advantages of our new technology, dynamic identification was also attempted with conventional modal analysis methods. A small steel beam with dimensions identical to the #1 specimen (single thickness, beam) was instrumented with two CEA-13-240UZ-120 strain gauges connected in half bridge configuration to a P-3500 strain indicator from Measurements Group, Inc. [34] The specimen was suspended in a free-free configuration and excited with a sharp impact. The resulting signal was collected with HP 54601B digital oscilloscope and processed numerically on a PC. Standard signal analysis algorithms (FFT) were used to extract the frequency spectrum. The first natural frequency (1.387 kHz) was clearly displayed.

The second natural frequency (3.789 kHz) could also be identified, but with a much weaker amplitude. These results are consistent with theoretical values and with the experimental results obtained with our new technology, as presented in Table 1. However, the impact excitation method was not able to excite the other higher frequencies depicted in Table 1, due, most probably, to bandwidth limitations inherent in impact excitation approach. We also considered the use of another conventional modal analysis method, specifically the sweep excitation method. In principle, sweep excitation would be able to reach all the natural frequencies within the sweep bandwidth. However, the application of this method to our small specimen was not found feasible due to attachment difficulties and the kHz range of frequency required that could not be easily achieved with conventional shakers. This demonstrates that, for the type of small rigid specimens as considered in our study, our proposed new technology has a niche of its own that cannot be filled by conventional modal analysis methods.

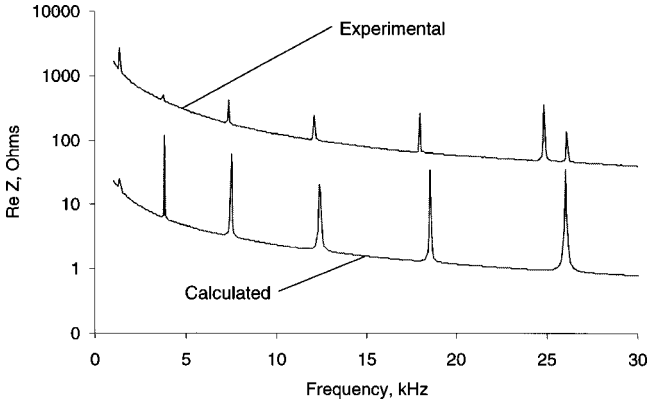

Fig. 8 Experimental and calculated spectra of frequencies for single thickness wide beam (Beam #3)

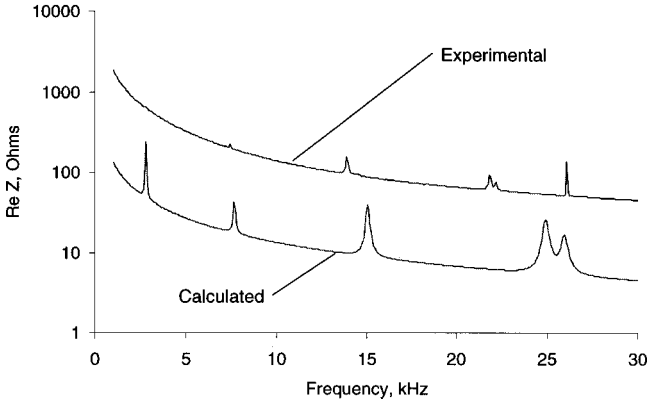

Fig. 9 Experimental and calculated spectra of frequencies for double thickness wide beam (Beam #4)

3.2 Sensor Calibration. In order to obtain consistent experimental results, a set of sensors was subject to a calibration procedure that consisted of geometrical measurement, electrical measurements and measurements of the intrinsic E/M impedance and admittance spectra of the PZT active sensors.

The results of the statistical analysis of geometrical data obtained showed small variations in dimensions from sensor to sensor. The mean and standard deviation values for length/width and thickness were 6.95 mm, ± 0.5 percent, and 0.224 mm, ± 1.4 percent, respectively. Electrical capacitance was measured as an in-process quality check to be applied during each step of sensor development and during the sensor installation process. Mean and standard deviation values were 3.276 nF, ± 3.8 percent, as it is shown on Fig. 10(*a*).

The intrinsic E/M impedance and admittance spectra of the PZT active sensors, before being attached to the structure, were measured with the HP 4194A Impedance Phase-Gain Analyzer. The PZT wafer was centered on the bold head and held in place with the probe tip. Thus, center clamping conditions were simulated, and the wafer could perform free vibrations while being tested. The statistical distributions of the resonance frequencies are given in Fig. 10(*b*). Mean values of 251 kHz and standard deviations of ± 1.2 percent were obtained. These results proved that the basic piezoelectric wafers had acceptable quality with a narrow dispersion band in resonance frequency. The detailed description on calibration process for piezoelectric active sensors could be found in Giurgiutiu and Zagrai, [35].

3.3 Noninvasive Characteristics of the Proposed Embedded Active Sensors. The active sensors used in the experiments were very small and did not significantly disturb the dynamic properties of the structure under consideration. Table 2 presents the mass and stiffness for the sensor and structure. For comparison, the mass of accelerometer is also presented [36].

The data and Table 2 illustrates numerically the noninvasive properties of piezoelectric wafer active sensors. The mass and stiffness additions brought by sensor are within the 1 percent range (0.5 percent for mass and 1.5 percent for stiffness). In spite of its small dimensions, the PZT wafer active sensor was able to adequately perform the dynamic structural identification of the test specimens, which is shown by results presented in Table 1 and a sequence of figures featured the E/M impedance spectrum of calculated and measured response. If the same identification were to be attempted with classical methodology, i.e., using an accelerometer and an impact hammer, the mass addition due to accelerometer would have been around 4.3 percent, which would greatly contaminate the results. This simple example underlines the fact that the use of piezoelectric wafer active sensors is not only advantageous, but in certain situations irreplaceable. For small com-

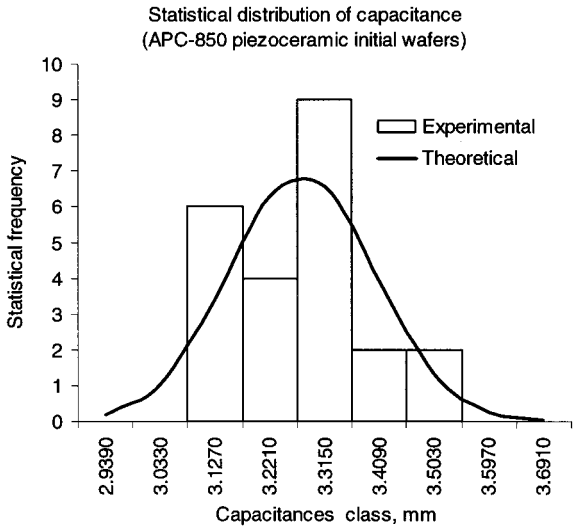

(*a*)

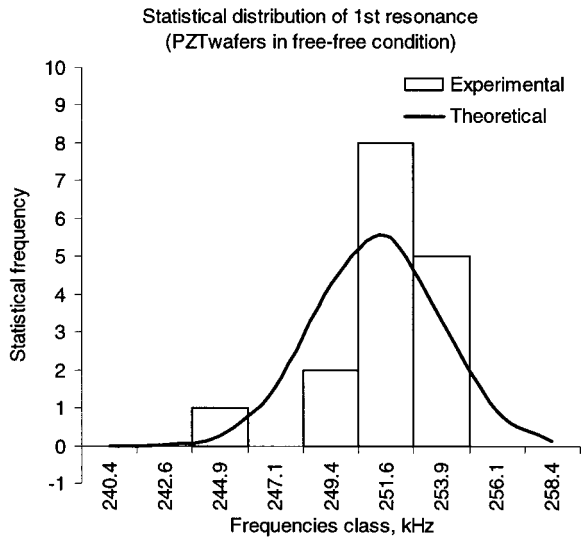

(*b*)

Fig. 10 Calibration results for piezoelectric wafer active sensors. Statistical distribution of: (*a*) capacitance as in-process quality check; (*b*) 1st resonance frequencies. (Solid line represents Gauss distribution.)

ponents such as in precision machinery and computer industry the use of PZT wafer active sensors could be the only practical option for insitu structural identification.

3.4 Active Sensor Self-Diagnostics. It is well known that piezo-electric wafer transducers affixed to, or embedded into, the structure play a major role in the successful operation of the health monitoring and damage detection system. Integrity of the transducer and consistency of the transducer/structure interface are essential elements that can ''make or break'' an experiment. The general expectation is that, once the transducers have been placed on or into the structure, they will behave consistently throughout the duration of the health monitoring exercise. For real structures, the duration of the health monitoring exercise is extensive and can span several years. It also will encompass various service conditions and several loading cases. Therefore, in-situ self-diagnostics methods are mandatory. The transducer array should be scanned periodically as well as prior to any damage detection cycle. Self-diagnostic methods for assessing active sensor integrity are readily available with the E/M impedance technique. The piezo-electric active sensor is predominantly a capacitive device that is dominated by its reactive impedance $1/i\omega C$.

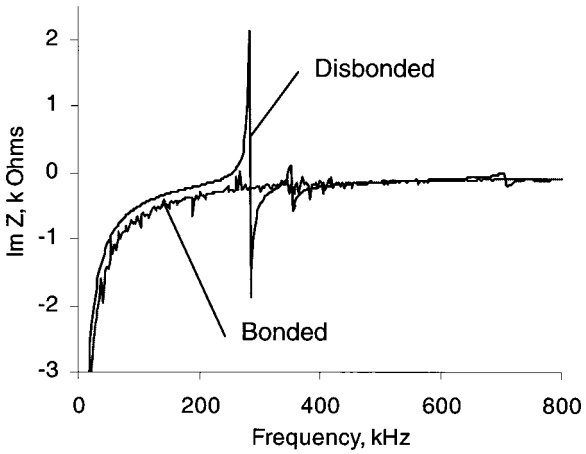

Fig. 11 Active sensor self-diagnostic using the imaginary part of the E/M impedance: when sensor is disbonded, new free-vibration resonance features appear at ~267 kHz

Our preliminary tests have shown that the reactive (imaginary) part of the impedance (Im Z) can be a good indication of active sensor integrity. Base-line signatures taken at the beginning of endurance experiments when compared with recent reading could successfully identify defective active sensors. Figure 11 compares the Im Z spectrum of a well-bonded PZT sensor with that of a disbonded (free) sensor. The appearance of sensor free-vibration resonance, and the disappearance of structural resonances constitute unambiguous features that can be used for automated sensor self-diagnostics.

3.5 Typical Applications. The piezoelectric active sensors and the associated structural dynamics identification methodology based on the electro-mechanical impedance response is ideally suited for small rigid machinery parts that have natural frequencies in the kHz range. As an example, we considered the aircraft turbo-engine blade presented in Fig. 12. Two PZT active sensors were installed, one on the blade, the other on the root. E/M impedance spectrum was recorded, and natural frequencies could be easily identified (Fig. 13).

Table 2 Numerical illustration of the noninvasive properties of the piezoelectric wafer active sensors

Sensor type	Mass, g	% of structural mass	Stiffness, MN/m	% of structural stiffness
Active sensor	0.082	0.5%	15	1.5%
Structure	16.4	N/A	1000	N/A
Accelerometer: 352A10, PCB Piezotronics [36]	0.7	4.3%	N/A	N/A

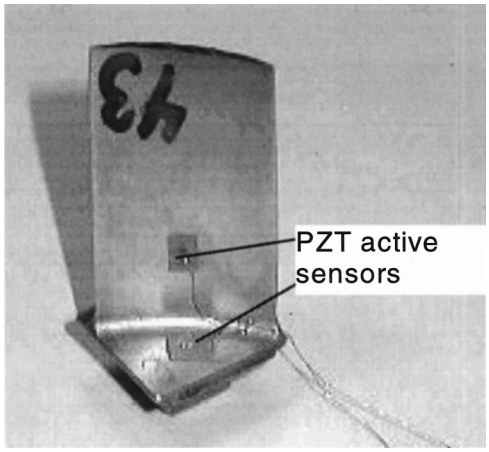

Fig. 12 Aircraft turbo-engine blade equipped with PZT active sensors

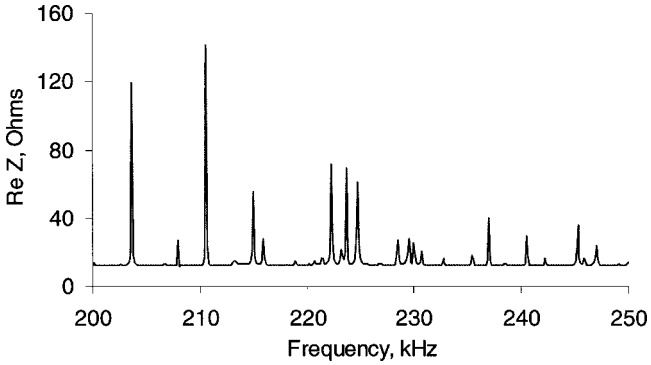

Fig. 13 E/M impedance spectrum of aircraft turbo-engine blade

4 Conclusions

The benefits and limitations of using embedded piezoelectric active sensors for structural identification at ultrasonic frequency are highlighted. An analytical model based on structural vibration theory and theory of piezoelectricity was developed and used to predict the electro-mechanical (E/M) impedance response, as it would be measured at the piezoelectric active sensor's terminals. The model considers one-dimension structures and accounts for both axial and flexural vibrations. Elastically-constrained piezoelectric active sensor permanently bonded to the structure were considered. The derived mathematical expressions accounted for the dynamic response of both the sensor and the structure. Experiments were conducted on simple specimens in support of the theoretical investigation, and on realistic turbine blade specimen to illustrate the method's potential. It was shown that E/M impedance spectrum recorded by the piezoelectric active sensors accurately represents the mechanical response of a structure. It was further proved that the response of the structure is not modified by the presence of the sensor, thus validating the latter's noninvasive characteristics. It is shown that such sensors, of negligible mass, can be permanently applied to the structure creating a nonintrusive sensor array adequate for on-line automatic structural identification and health monitoring. The sensor calibration procedure was presented. Numerical estimation of the noninvasive properties of the proposed active sensors in comparison with conventional sensors is presented. Self-diagnostics capabilities of the proposed sensors were also investigated and methods for automatic self-test implementation are discussed. As presented in this paper, the proposed method, using just one active sensor, can only detect structural resonances. The detection of structural mode shapes is also possible, but requires the simultaneous use of several sensors, their number being in direct relationship to the desired modal resolution.

A limitation of the proposed technology is that, by being tuned to high frequency explorations, it does not behave well below 5 kHz. These difficulties can be alleviated in the 1–5 kHz range by narrowband tuning, and this was done during the experiments reported here. However, below 1 kHz, the method is simply not recommended.

In view of these advantages and disadvantages, it is felt that piezoelectric active sensors in conjunction with the E/M impedance technique, have their niche as a structural identification methodology using self-sensing, permanently attached active sensors. Due to their perceived low cost (<$10), these active sensors can also be inexpensively configured as sensor arrays. The proposed method can be a useful and reliable tool for automatic on-line structural identification in the ultrasonic frequencies range. The use of piezoelectric-wafer active sensors cannot only be advantageous, but, in certain situations, may be the sole investigative option, as in the case of precision machinery, small but critical turbine-engine parts, and computer industry components.

Acknowledgments

The financial support of the Department of Energy through the Sandia National Laboratories, contract doc. #BF 0133 is thankfully acknowledged. Sandia National Laboratories is a multiprogram laboratory operated by Sandia Corporation, a Lockheed Martin Company, for the United States Department of Energy under contract DE-AC04-94AL85000.

References

[1] Harris, C., M., 1996, *Shock and Vibration Handbook*, McGraw-Hill, NY.
[2] Ewins, D. J., 1984, *Modal Test: Theory and Practice*, Research Studies Press Ltd., Letchworth, Hertfortshire, England.
[3] Maia, N., Silva, J., He, J., Lieven, N., Lin, R., Skingle, G., To, W., and Urgueira, A., 1997, *Theoretical and Experimental Modal Analysis*, Research Studies Press Ltd.
[4] Heylen, W., Lammens, S., and Sas, P., 1997, *Modal Analysis theory and Testing*, Katholieke Universiteit Leuven, Heverrlee, Belgium.
[5] Broch, J. T., 1984, Mechanical Vibration and Shock Measurements, Brüel & Kjaer.
[6] Polytec PI, Inc., 2000, www.polytecpi.com.
[7] Crawley, E. A., and deLuis, J., 1987, "Use of Piezoelectric Actuators as Elements of Intelligent Structures," AIAA J., **25**, No. 10, pp. 1375–1385.
[8] Dimitriadis, E. K., Fuller, C. R., and Roger, C. A., 1991, "Piezoelectric Actuators for Distributed Vibration Excitation of Thin Plates," ASME J. Vibr. Acoust., **113**, pp. 100–107.
[9] D'Cruz, J., 1993, "Active Control of Panel Vibrations with Piezoelectric Actuators," J. Intell. Mater. Syst. Struct., **4**, No. 3, Jul 93, p. 398–402.
[10] Zhou, S., Liang, C., and Rogers, C., 1996, "An Impedance-Based System Modeling Approach for Induced Strain Actuator-Driven Structures," ASME J. Vibr. Acoust., July 96, pp. 323–331.
[11] Collins, K., Plau, R., and Wauer, J., 1992, "Free and Forced Longitudinal Vibrations of Cantilevered Bar with a Crack," ASME J. Vibr. Acoust., **114**, pp 171–177.
[12] Clark, R. L., Burdisso, R A., and Fuller, C. R., 1993 "Design Approaches for Shaping Polyvinylidene Fluoride Sensors in Active Structural Acoustic Control," J. Intell. Mater. Syst. Struct., **4**, No. 3, Jul, pp. 354–365.
[13] Banks, H. T., Smith, R. C., and Wang, Y., 1996, *Smart Material Structures: Modeling, Estimation and Control*, Masson, John Wiley & Sons, Paris.
[14] Wang, B., and Chen, R., 2000, "The Use of Piezoceramic Transducers for Smart Structural Testing," *Proceedings of SPIE 2000 Conference*, Newport Beach, CA.
[15] Lian, C., Sun, F. P., and Roger, C. A., 1994, "Coupled Electro-Mechanical Analysis of Adaptive Material System-Determination of the Actuator Power Consumption and System energy Transfer," J. Intell. Mater. Syst. Struct., **5**, January, pp. 12–20.
[16] Sun, F. P., Liang, C., and Rogers, C. A., 1994, "Experimental Modal Testing Using Piezoceramic Patches as Collocated Sensors-Actuators," *Proceedings of the 1994 SEM Spring Conference & Exhibits*, Baltimore, MI, June 6–8.
[17] Chaudhry, Z., Sun, F. P, and Rogers, C. A., 1994, "Health Monitoring of Space Structures Using Impedance Measurements," *Fifth International Conference on Adaptive Structures*, Sendai, Japan December 5–7, pp. 584–591.
[18] Chaudhry, Z., Joseph, T., Sun, F., and Rogers, C., 1995, "Local-Area Health Monitoring of Aircraft via Piezoelectric Actuator/Sensor Patches," *Proceed-*

ings, SPIE North American Conference on Smart Structures and Materials, San Diego, CA, March, Vol. 2443, pp. 268–276.
[19] Ayres, T., Chaudhry, Z., and Rogers, C., 1996, ''Localized Health Monitoring of Civil Infrastructure via Piezoelectric Actuator/Sensor Patches,'' *Proceedings, SPIE 1996* Symposium on Smart Structures and Integrated Systems, SPIE, Vol. 2719, pp. 123–131.
[20] Giurgiutiu, V., Reynolds, A., and Rogers, C. A., 2000, ''Experimental Investigation of E/M Impedance Health Monitoring of Spot-Welded Structural Joints,'' J. Intell. Mater. Syst. Struct., **10**, No. 10, October, pp. 802–812.
[21] Park, G., Cudney, H. H., Inman, D. J., 2000, ''An Integrated Health Monitoring Technique Using Structural Impedance Sensors,'' J. Intell. Mater. Syst. Struct., **11**, No. 6, June, pp. 448–455.
[22] Wang, B., and Rogers, C.A., 1991, ''Modeling of Finite-Length Spatially-Distributed Induced Strain Actuators for Laminate Beams and Plates,'' Proccedings *AIAA/ASME/ASCE/AHS/ASC* 32*nd Structures, Structural Dynamics, and Material Conference*.
[23] Esteban, J., 1996, ''Analysis of the Sensing Region of a PZT Actuator-Sensor,'' Ph.D. Dissertation, Virginia Polytechnic Institute and State University, July.
[24] Graff, K. F., 1975, *Wave Motion in Elastic Solids*, Dover Publications, Inc.
[25] IEEE Standard on Piezoelectricity, 1987, *An American National Standard*, The Institute of Electrical and Electronics Engineers, Inc.
[26] Ikeda, T., 1996, *Fundamentals of Piezoelectricity*, Oxford Science Publications.
[27] Giurgiutiu, V., Chaudhry, Z., and Rogers, C. A., 1994, ''The Analysis of Power Delivery Capability of Induced Strain Actuators for Dynamic Applications,'' *Proceedings of the Second International Conference on Intelligent Materials, ICIM'94*, June 5–8, Colonial Williamsburg, VA, Technomic Pub. Co., Inc., pp. 565–576.
[28] Giurgiutiu, V., and Rogers, C. A., 1997, ''Electro-Mechanical (E/M) Impedance Method for Structural Health Monitoring and Non-Destructive Evaluation,'' *International Workshop on Structural Health Monitoring, Stanford University*, CA, September 18–20, pp. 433–444.
[29] Timoshenko, S. P., 1955, *Vibration Problems in Engineering*, D. Van Nostrand Company Inc.
[30] Meirovitch, L., 1986, *Elements of Vibration Analysis*, 2nd edition, McGraw-Hill.
[31] Inman, D. J., 1996, *Engineering Vibration*, Prentice-Hall, Inc.
[32] Kelly, S. G., 2000, *Fundamentals of Mechanical Vibration*, 2nd edition, McGraw-Hill.
[33] Blevins, R. D., 1979 *Formulas for Natural Frequency and Mode Shape*, Litton Educational Publishing Inc.
[34] Measurements Group, Inc., P.O. Box 27777, Raleigh, NC 27611, (www.measurementsgroup.com).
[35] Giurgiutiu, V., and Zagrai, A., 2000, ''Damage Detection in Simulated Aging-Aircraft Panels Using the Electrico-Mechanical Impedance Technique,'' *Adaptive Structure and Material Systems Symposium*, ASME Winter annual meeting, Nov. 5–10, Orlando, FL.
[36] PCB Piezotronics, 1999, www.pcb.com.